AD-A153 636 DESIGN CONSIDERATION FOR THE X-RAY CERENKOV EXPERIMENT 1/1
(U) NAVAL POSTGRADUATE SCHOOL MONTEREY CA Y D CHOI
DEC 84

UNCLASSIFIED F/G 20/9 NL

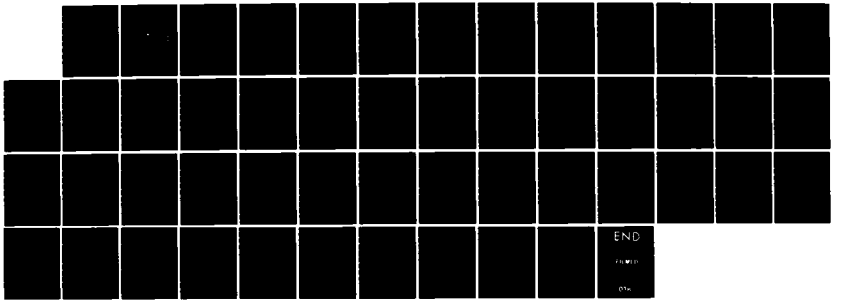

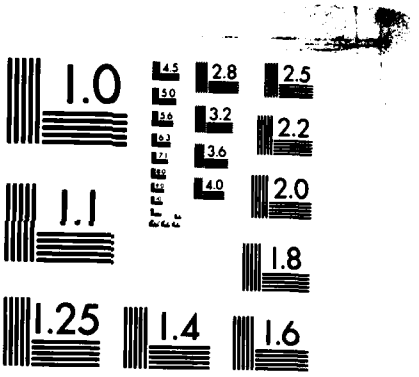

(2)

NAVAL POSTGRADUATE SCHOOL

Monterey, California

THESIS

DESIGN CONSIDERATION
FOR THE X-RAY CERENKOV EXPERIMENT

by

Youn Dae Choi

December 1984

Thesis Advisor: John R. Neighbours

Approved for public release; distribution is unlimited.

85 [illegible] 9

SECURITY CLASSIFICATION OF THIS PAGE (When Data Entered)

REPORT DOCUMENTATION PAGE		READ INSTRUCTIONS BEFORE COMPLETING FORM
1. REPORT NUMBER	2. GOVT ACCESSION NO. AD-A153 636	3. RECIPIENT'S CATALOG NUMBER
4. TITLE (and Subtitle) Design Consideration for the X-ray Cerenkov Experiment		5. TYPE OF REPORT & PERIOD COVERED Master's Thesis; December 1984
		6. PERFORMING ORG. REPORT NUMBER
7. AUTHOR(s) Youn Dae Choi		8. CONTRACT OR GRANT NUMBER(s)
9. PERFORMING ORGANIZATION NAME AND ADDRESS Naval Postgraduate School Monterey, California 93943		10. PROGRAM ELEMENT, PROJECT, TASK AREA & WORK UNIT NUMBERS
11. CONTROLLING OFFICE NAME AND ADDRESS Naval Postgraduate School Monterey, California 93943		12. REPORT DATE December 1984
		13. NUMBER OF PAGES 49
14. MONITORING AGENCY NAME & ADDRESS(if different from Controlling Office)		15. SECURITY CLASS. (of this report)
		15a. DECLASSIFICATION/ DOWNGRADING SCHEDULE

16. DISTRIBUTION STATEMENT (of this Report)

Approved for public release; distribution is unlimited.

17. DISTRIBUTION STATEMENT (of the abstract entered in Block 20, if different from Report)

18. SUPPLEMENTARY NOTES

19. KEY WORDS (Continue on reverse side if necessary and identify by block number)

Cerenkov Radiation; X-ray; Proportional Counter.

20. ABSTRACT (Continue on reverse side if necessary and identify by block number)

The feasability of measuring Cerenkov radiation in the X-ray region has been investigated. It is found that the experimental measurement of X-ray Cerenkov radiation is possible for the carbon K (283.84eV), aluminum L1 (87.01 eV) and L2,3 (72.78 eV) absorption edges. Measurement in the aluminum K (1559.9 eV) absorption edge region is found to be not possible since the real part of the index of refraction does not exceed unity. The relative power from Cerenkov radiation has been calculated for

DD FORM 1 JAN 73 1473 EDITION OF 1 NOV 65 IS OBSOLETE

S/N 0102-LF-014-6601

SECURITY CLASSIFICATION OF THIS PAGE (When Data Entered)

the three possible cases and count rate estimates are given. The experimental apparatus for the measurement of X-ray Cerenkov radiation has been redesigned to allow measurement of the carbon K edge and aluminum L1 edge.

An experiment was attempted, but not completed due to the failure of a necessary preamplifier for a proportional counter. New design considerations are presented here and incorporate changes to avoid the experimental shortcomings of previous measurements.

Approved for public release; distribution is unlimited.

Design Consideration
for the X-ray Cerenkov Experiment

by

Youn Dae Choi
Major, Republic of Korea Army
B.S., Korea Military Academy, 1976
B.S., Kyung Puk National University, 1980

Submitted in partial fulfillment of the
requirements for the degree of

MASTER OF SCIENCE IN PHYSICS

from the

NAVAL POSTGRADUATE SCHOOL
December 1984

Author: Choi, Youn Dae
Youn Dae Choi

Approved by: John R Neighbours
John R. Neighbours, Thesis Advisor

Xavier K. Maruyama
Xavier K. Maruyama, Second Reader

G E Schacher
Gordon E. Schacher,
Chairman, Department of Physics

J. N. Dyer
John N. Dyer,
Dean of Science and Engineering

ABSTRACT

The feasability of measuring Cerenkov radiation in the X-ray region ~~has been~~ was investigated. It is found that the experimental measurement of X-ray Cerenkov radiation is possible for the carbon K (283.84 eV), aluminum L1 (87.01 eV) and L2,3 (72.78 eV) absorption edges. Measurement in the aluminum K (1559.9 eV) absorption edge region ~~is~~ was found to be not possible since the real part of the index of refraction ~~does~~ did not exceed unity. The relative power from Cerenkov radiation ~~has been~~ was calculated for the three possible cases and count rate estimates ~~are~~ were given. The experimental apparatus for the measurement of X-ray Cerenkov radiation ~~has been~~ was redesigned to allow measurement of the carbon K edge and aluminum L1 edge.

An experiment was attempted, but not completed due to the failure of a necessary preamplifier for a proportional counter. New design considerations ~~are~~ were presented ~~here~~ and incorporated changes to avoid the experimental shortcomings of previous measurements.

cont Keywords include: see 1473

TABLE OF CONTENTS

LIST OF TABLES

LIST OF FIGURES

ACKNOWLEDGEMENTS

I would like to express my gratitude and appreciation to Professor John R. Neighbours and Professor Xavier K. Maruyama for guidance, advice and corrections throughout this research.

Also, I want to thank Mr. D. Snyder for the Linac operation and many others who have contributed much before the last page of this paper was written.

Youn Dae Choi

I. INTRODUCTION

Cerenkov radiation is produced by a charge or a group of charges moving at speeds greater than light in a particular medium. It has been investigated with the experiments of Cerenkov in 1934 and also described by Frank and Tamm in 1937. A summary of work to 1958 is contained in the treatise by Jelly [Ref. 1].

Cerenkov radiation has been used occasionally as a detector of high speed charged particles. A detector using this concept will selectively detect only charged particles exceeding the velocity of light in the medium through which they are traveling. Other than this it has been considered as a curiosity, and the phenomenon has been usually thought to be a source of broadband radiation.

Until recently the study of Cerenkov radiation has been restricted almost exclusively to radiation in the optical region, and most theoretical and experimental studies have been devoted to the properties of Cerenkov radiation in the optical band where photoabsorption effects can usually be ignored. This was due to the belief that Cerenkov radiation in the X-ray band is impossible since the index of refraction of all media is less than unity over the X-ray frequency region.

The velocity of light in a medium is equal to c_o/n, where c_o is the velocity of light in vacuum, n the index of refraction of the medium, and the index of refraction in the X-ray region is of the form :

$$n(\omega) = \left[1 - \frac{\omega_p^2}{\omega^2}\right]^{\frac{1}{2}} \qquad (1.1)$$

where ω_p is the plasma frequency of the electrons of the medium. This was the accepted theory. Recently, Bazylev

et. al. [Ref. 3] reported the observation of Cerenkov radiation from carbon at wavelength of 40 angstroms using 1.2 GeV electrons. The experiment was based on a theory that near the photoabsorption edges the coupling of the electrons with the atoms of the medium alters the index of refraction, resulting in narrow bands where the real part of the index of refraction is greater than unity.

In this thesis, three sets of experiments which could be performed by using Naval Postgraduate School 100 MeV Linac are discussed. They utilize absorption edges as follows:

1. Carbon K (283.84 eV).
2. Aluminum L1 (87.01 eV) and L2,3 (72.78 eV).
3. Aluminum K (1559.9 eV).

The purpose of this thesis is to understand the characteristics of Cerenkov radiation and to see if X-ray Cerenkov radiation can be emitted in another medium in accordance with the theory, and possible detection methods for soft X-rays are discussed.

II. THEORY

A. CHARACTERISTICS OF CERENKOV X-RADIATION

A charged particle in uniform motion in a straight line in free space does not radiate. The situation may be different, however, in a dielectric medium for which $\varepsilon > \varepsilon_0$, $K>1$, and index of refraction of the medium, n, can be written as:

$$n = \left[\frac{\varepsilon}{\varepsilon_0}\right]^{\frac{1}{2}} = \left[K\right]^{\frac{1}{2}} \qquad (2.1)$$

where ε_0 is the permittivity of free space, ε the permittivity of the medium, and K the dielectric constant of the medium.

If the electron is moving fast, that is, at a velocity comparable to that of light in the medium, there is a resultant dipole field which will be apparent even at large distances from the track of the electron. Such a field will be momentarily set up by the electron at each line element along the track, and in turn each molecule in the line element will then radiate a brief electromagnetic pulse. The radiation will be spread over a band of frequencies corresponding to the various Fourier components of this pulse.

In the general case, the radiated wavelets from all parts of the track interfere destructively so that, at a distant point, the resultant field intensity is still zero. However, if the velocity of the particle is greater than the phase velocity of the radiated wave in the medium, it is possible for the wavelets from all portions of the track to be in phase with one another so that, at a distant point of observation, there is now a resultant field. It will be

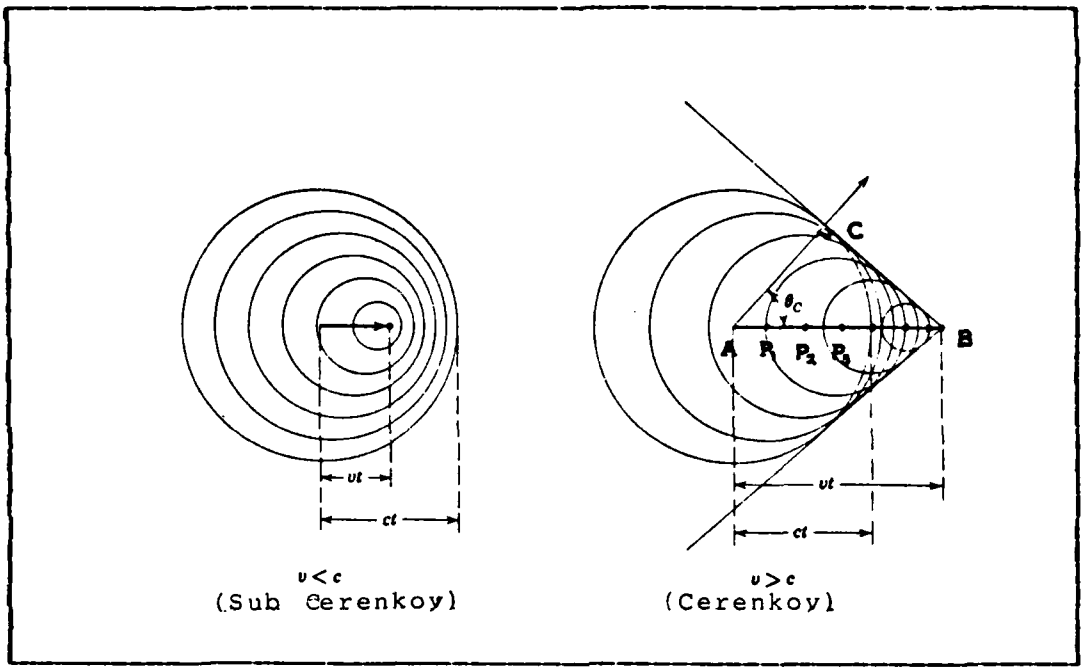

Figure 2.1 Huygens Construction of Wavelet for Cerenkov Radiation.

understood from the Huygens construction shown in Figure 2.1 that this radiation is only observed at a particular angle θ_c with respect to the track of the particle, namely that angle at which the wavelets from arbitary points such as P1, P2 and P3 on the track AB are coherent and combine to form a plane wave front, BC. This coherence takes place when the particle traverses AB in the same time that the light wave travels from A to C. If β is defined as v/c_o where v is the velocity of the particle, then in a time t the particle will travel a distance AB = $\beta c_o t$ and the light will travel a distance AC = $(c_o/n).t$. From this geometry we obtain

$$\cos \theta c = 1/n\beta \qquad (2.2)$$

which is known as the Cerenkov relation, where θc is the direction of emission of the Cerenkov radiation.

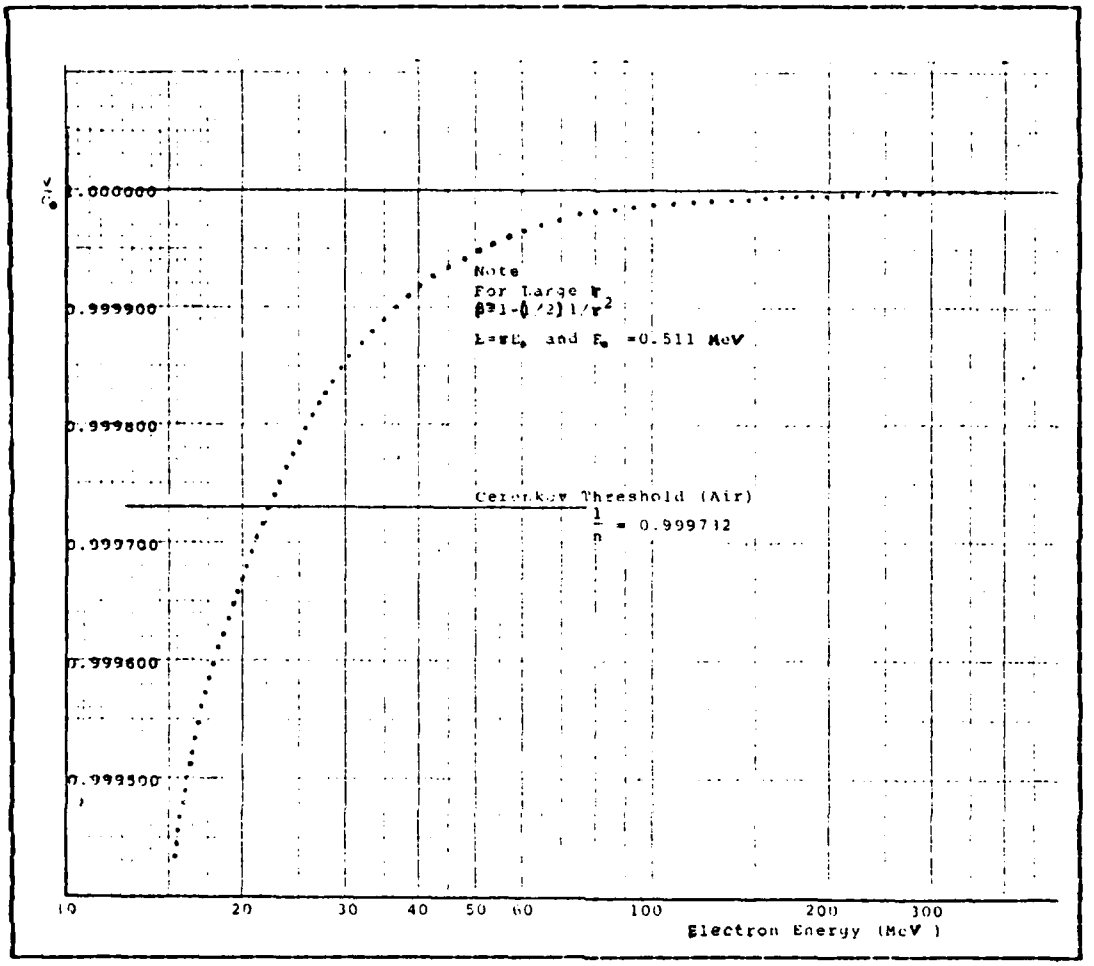

Figure 2.2 Electron Energy vs. 1/n (=v/c).

It is seen that:

1. For a medium of given refractive index, n, there is a threshold velocity $\beta_{min} = 1/n$, below which no radiation take place. Figure 2.2 shows a relationship between β (i.e., v/c) and electron energy in MeV. Note that, in the case of air, 1/n = 0.999732, to achieve Cerenkov radiation the electron energy needs to be greater than 22 MeV. At this critical velocity(energy) the direction of radiation coincides with that of the particle.

2. For an ultra-relativistic particle, for which $\beta \cong 1$, there is a maximum angle of emission, given by $\theta_c max = \cos^{-1}(1/n)$.
3. The radiation occurs mainly in the visible and near-visible regions of the spectrum, for which $n>1$. Emission in the X-ray region is relatively hard to produce for n is less than unity in most of the region and thus equation (2.2) can not be satisfied except near photoabsorption edges.

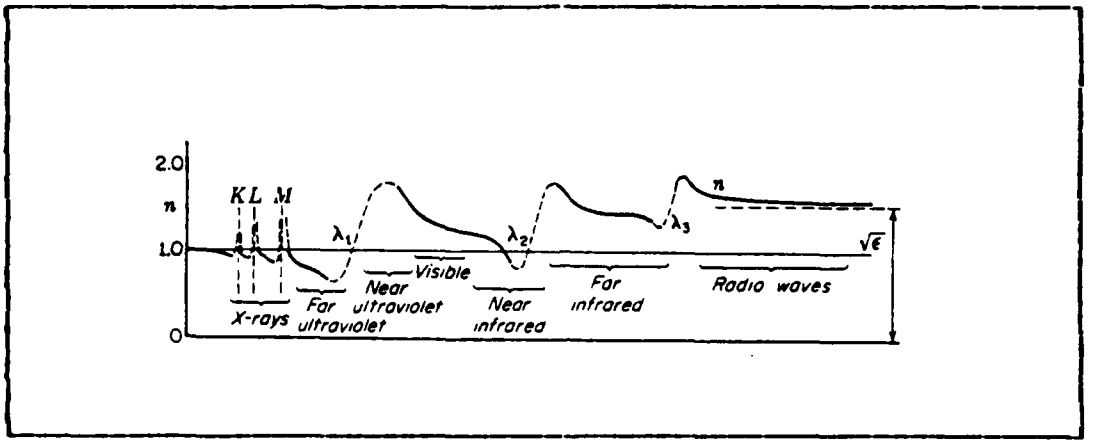

Figure 2.3 The Dispersion Curve of a Typical Medium.

In order to achieve Cerenkov X-radiation, the index of refraction of the target material must be greater than unity, which occurs only at the absorption edges (see Figure 2.3, which shows the schematic diagram of a complete dispersion curve for a substance transparent to the visible spectrum). Since emission of X-ray Cerenkov radiation is only possible in regions close to absorption lines and bands, and the deviation from unity turns out to be relatively small, the incident particle energy must be relativistic, and the radiation angle turns out to be quite small. In this case the theory used to describe dispersionless optical Cerenkov

radiation appears, generally speaking, inapplicable. Therefore, there exists a need to develop a theory based on the effect of the absorbing properties of the medium.

B. INDEX OF REFRACTION IN THE X-RAY REGION

The Cerenkov angle, θ_c, can be computed from equation (2.2) assuming that the electron is moving at constant velocity, v.

Classically, the atoms of the medium can be modeled as an oscillator consisting of an electron of mass m vibrating about a massive positive charge, which we may consider to be at rest, and on which falls an electromagnetic wave of angular frequency ω, whose electric vector at the position of the dipole is given at time t by:

$$\vec{E} = \vec{E}_0 \, \mathrm{Exp}(i\omega t) \qquad (2.3)$$

We assume that $\vec{E}$ and the induced dipole moment $\vec{P}$ depend on position and time sinusoidally, or have a complex form ('^' represents complex). The equation of motion of the electron under the action of the wave is:

$$\ddot{\vec{x}} + (k/m)\dot{\vec{x}} + \omega_s^2 \vec{x} = (e\vec{E}_0/m) \, \mathrm{Exp}(i\omega t) \qquad (2.4)$$

In this equation, a damping factor k, proportional to the velocity of the displaced charge, has been introduced, and ω_s is the natural frequency of the dipole if the charge is displaced and allowed to oscillate without either applied field or damping. When a steady state has been reached, the dipole executes forced oscillations of frequency ω under the action of the incident wave, with a dipole moment at time t being given by:

$$\vec{P} = e\vec{x} = (e^2/m) \frac{\vec{E}_0 \, \mathrm{Exp}(i\omega t)}{\omega_s^2 - \omega^2 + iK\omega} \qquad (2.5)$$

which can be verified by direct substitution in equation (2.4).

Now f, the scattering factor (for more details see [Ref. 5]) of the dipole is defined as the ratio of the amplitude scattered by the oscillator to that scattered by a free classical electron under the same conditions. We get for f, the scattering factor of a dipole oscillator of natural frequency ω_s, for waves of frequency ω,

$$f = \frac{\omega^2}{\omega_s^2 - \omega^2 + ik\omega} \qquad (2.6)$$

f can be written as:

$$f = f1 + if2 \qquad (2.7)$$

These are the real and imaginary parts of the response function (or f) assuming that the electron behaves like a classical harmonic oscillator. The general result for the relation between the real and imaginary parts of the response function (or f) is derived from causality arguments and is called the Kramers-Kronig relation in physics. These relations are used to obtain that part of the response function which is difficult to measure directly. In the case of the optical constants in the X-ray region the Kramers-Kronig relations are used to obtain the index of refraction from measurements of the absorption. The functions f1 and f2 are tabulated by Henke et al [Ref. 5] for low energy X-rays from 100 eV to 2000 eV for 94 elements. Figure 2.4 represents a plot of f1, f2 versus X-ray energy for the case of carbon, and Figure 2.5 shows a plot of f1, f2 versus X-ray energy for the case of alumnium.

For X-rays, the real part of the index of refraction, n, is given in terms of the scattering factor f1 by :

$$n = 1 - \frac{N e^2}{\varepsilon_0 m \omega^2} f1 \qquad (2.8)$$

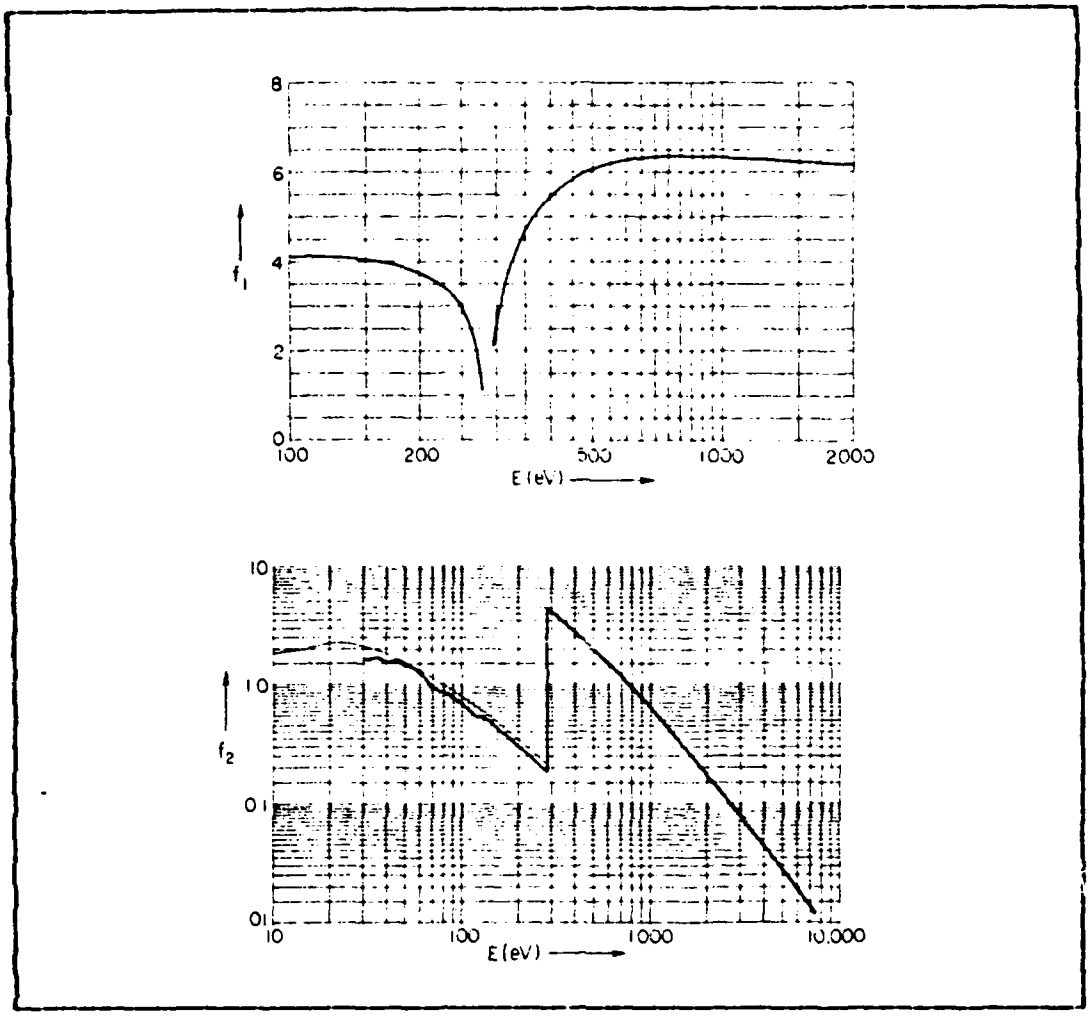

Figure 2.4 Atomic Scattering Factors of Carbon.

and the imaginary part of the index of refraction, k, is given in terms of the scattering factor f2 by:

$$k = \frac{N e^2}{\varepsilon_0 m \omega^2} f2 \qquad (2.9)$$

where N is the number of atoms per cubic meter, e the electron charge in coul, and m the electron mass in Kg. From Figure 2.4 and Figure 2.5 and equation (2.8), in order for n to be greater than unity in the X-ray frequency region, f1

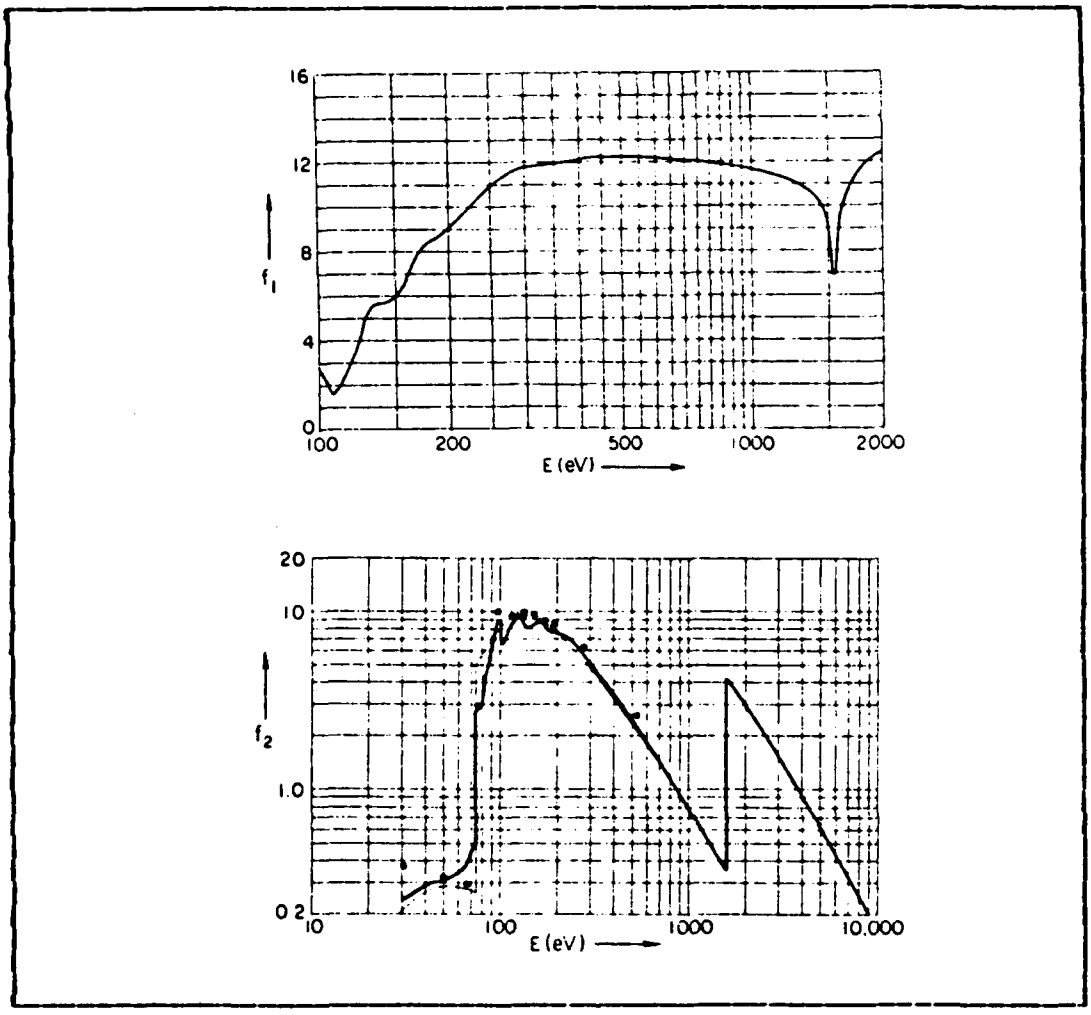

Figure 2.5 Atomic Scattering Factors of Aluminum.

must have negative values. This occurs in very narrow bands where apparently f1 was not calculated by Henke and his coworkers.

A more rigorous calculation of the index of refraction, near the photoabsorption edges, however, has lead to results different from those implied by Figure 2.4 and Figure 2.5 D.Y Smith et al [Ref. 6] used a finer mesh of points(500) to obtain the optical constants of aluminum. The actual

calculations were carried out in terms of the complex dielectric constant

$$\hat{K}(\omega) = Kr(\omega) + i\, Ki(\omega) \qquad (2.10)$$

The elastic part of the dielectric constant Kr was obtained from the absorptive part using the Kramers-Kronig relation

$$Kr(\omega) - 1 = \frac{2}{\pi} \int_0^\infty \frac{\omega' Ki(\omega')\, d\omega'}{\omega'^2 - \omega^2} \qquad (2.11)$$

and the desired optical constants were then computed from the complex dielectric constant

$$n = \left[\frac{1}{2}(K_r + \sqrt{K_r^2 + K_i^2})\right]^{\frac{1}{2}} \qquad (2.12)$$

$$k = \left[\frac{1}{2}(-K_r + \sqrt{K_r^2 + K_i^2})\right]^{\frac{1}{2}} \qquad (2.13)$$

Figure 2.6 shows the optical constants of aluminum over 4 decades of energy and Table I shows the value of the constants near L1, L2,3 and K edges. As we can see from the

TABLE I

Optical Properties of Aluminum

Absorption Edges	Energy in eV	Real Part (n)	Imaginary Part (k)
L1	86	1.0059	0.028233
	87	1.0055	0.028496
	88	1.0054	0.028958
L2,3	72.6	1.03	0.00395
	72.7	1.0339	0.012328
	72.8	1.0302	0.019984
K	1558	0.99992	0.000029
	1559	0.99992	0.000033
	1560	0.99992	0.000041

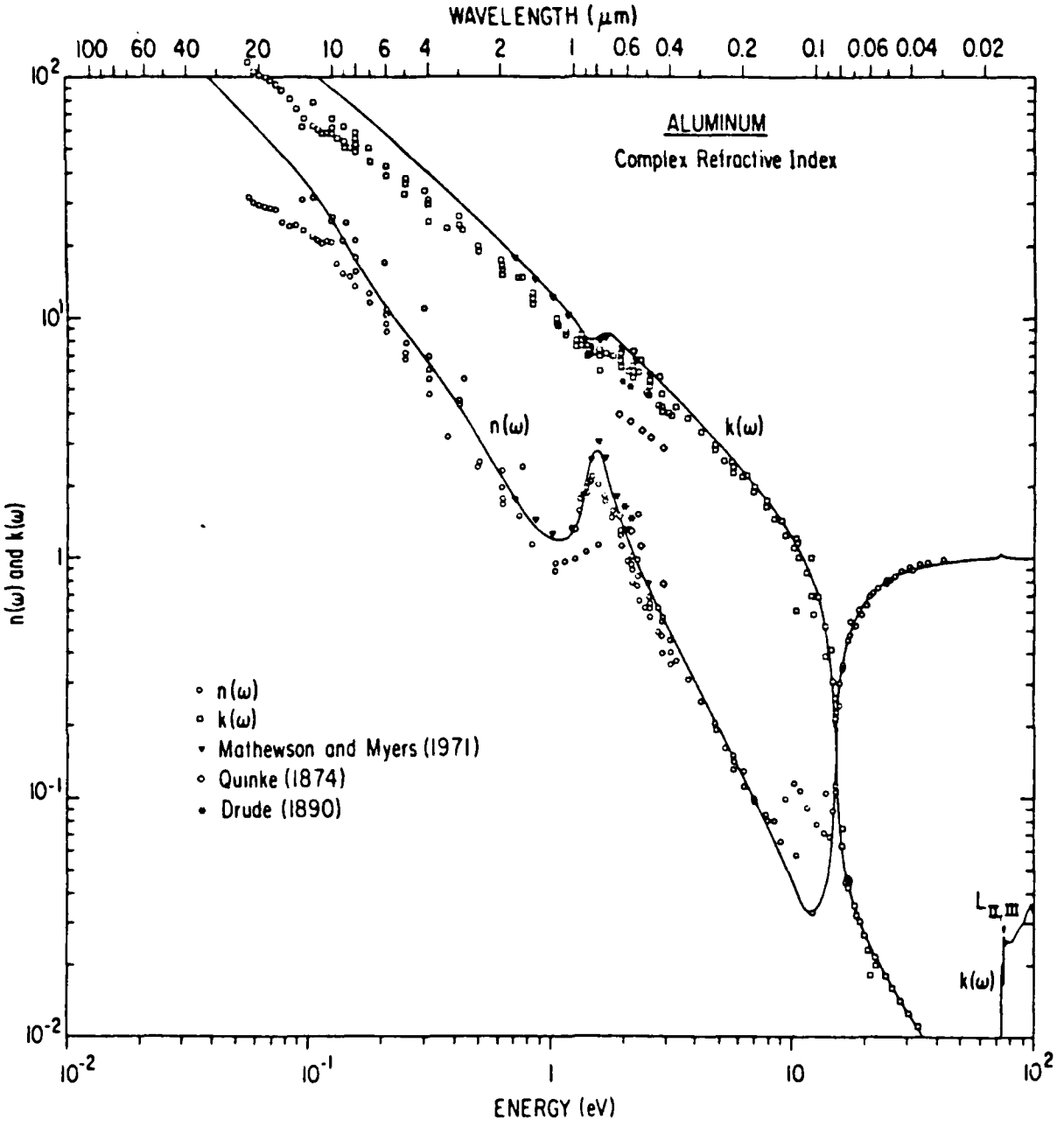

Figure 2.6 The Refractive Index of Metallic Aluminum.

Table I and Figure 2.6, the index of refraction near L1 and L2,3 edges are slightly higher than unity (notice a little hump near the L2,3 edge in Figure 2.6) but near the K edge is still less than unity for the case of aluminum.

An X-ray Cerenkov radiation experiment in the aluminum K edge region by Farmer [Ref. 8] was not able to be repeated and the reasons at that time were not known. It is evident from Table I that realistic value of the index of refrection [Ref. 6] does not exceed unity near the K absorption edge of aluminum. For this reasion the results of Farmer must be viewed not as a measurement but as a first attempt to do this type of experiment.

With the above in mind, an examination is given to the real part of the index of refraction near the photoabsorption edges of the various shells of an atom. The relation between the real and imaginary parts of the index of refraction, through the dispersion relation of Kramers-Kronig relation, gives rise to the absorption that electrons with binding energies exceeding the photon energy will add a positive contribution to the real part of the index of refraction of the medium. At the same time, electrons whose binding energies are less than that of the photon will cause a negative contribution. The requirement is to find a media in which the positive contributions are larger than the negative ones in some X-ray frequency regions such that the index of refraction is greater than unity. As a result of the fine structure of the photcabsorption edges due to the transitions of the electrons to valence level, detailed experimental data on the photoabsorption cross section must be utilized in determining the real and imaginary parts of the index of the refraction. The real part of the index of refraction turns out to be greater than unity in a relatively narrow interval of the sought X-ray frequency band. However, within this frequency interval, the real part of the index of refraction does exceed unity, allowing the formation of Cerenkov radiation in the band.

C. RADIATED POWER

F.R Buskirk and J.R Neighbours [Ref. 7] calculated the radiation power from periodic electron bunches, by considering the Cerenkov radiation produced in a dispersionless medium such as gases or other dielectrics by a series of pulses of electrons such as are produced by a Linac. The pulses or bunches are assumed periodic. The total emission region is finite, and the bunches have a finite size. From this, the average power per unit solid angle radiated at the frequency ω, which is a harmonic of the basic angular frequency ω_0 of the periodic pulse train, is:

$$dP/d\Omega = \sum_{\omega=0}^{\infty} W\ (\omega, \hat{n}) \qquad (2.14)$$

For convenience $W(\nu, \hat{n})$ can be written below using slightly different terminology:

$$W\ (\nu, \hat{n}) = \frac{Mc^2 \mu^2 q^2}{8\pi^2} \left|F(\vec{k})\right|^2 \left[(kL)^2 \sin^2\theta\, I^2(u)\right] \qquad (2.15)$$

where $W\ (\nu, \hat{n})$ is the power per unit solid angle radiated at the frequency $\nu = c\vec{k}/2\pi$. The parameters describing the radiation are:

$$u = kL/2\ (\cos\theta_c - \cos\theta) \qquad (2.16)$$

$$I(u) = \sin u / u \qquad (2.17)$$

$$k = (n_x\ \omega/c,\ n_y\ \omega/c,\ \omega/c) \qquad (2.18)$$

$$\hat{\rho}_o'(\vec{k}) = \iiint_{-\infty}^{\infty} dx\, dy\, dz\ \mathrm{Exp}[-i\vec{k}\cdot\vec{r}]\, \rho_o'(\vec{r}) \qquad (2.19)$$

$$= q\ F(\vec{k})$$

where n_x, n_y, n_z are components of the unit vector $\hat{n}$ in the emission direction, ν is the frequency of the emitted radiation, L $(= 2Z')$ is the length of the medium, and the usual Cerenkov angle θ_c is given by $\cos\theta c = c/v$. The total charge of one bunch is q, corresponding to a charge distribution

$\rho'(\vec{r})$ with Fourier transform $\tilde{\rho}'(\vec{k}) = qF(\vec{k})$, and $F(\vec{k})$ is defined as a dimensionless form factor. The Linac frequency ν_o is equal to the electron velccity divided by the electron bunch spacing Z ($\nu_o = v/Z$), and ν, the frequency of the emitted radiation will be a harmonic of ν_o.

In equation (2.15), the quantity enclosed in square brackets is a dimensionless radiation function. The factor $I^2(u)$ is identical to the result obtained for the calculation of elementary Fraunhofer diffraction from a slit across which the phase varies linearly, such as plane waves striking the slit at an angle to the normal. To calculate and plot expected results, a set of parameters were chosen close to those available in an experimental situation:

1. The index of refraction for carbon at the K edge is 1.003379. The electron parameters are assumed to be those for a 100 MeV Linac; fundamental frequency ν_o = 2.856 GHz, and form factcr is assumed to be 1. Since the radiation emerging from the target actually orginates at the last layer having a thickness on the order of the absorption length ($l_c = \frac{\lambda}{\epsilon''}$) or 1.1 μm for carbon target, and assuming e^{-1} of the absorption length contributes to the radiation, the radiation length of the medium is 0.40 micrometers.
2. The index of refraction for the aluminum L2,3 edge is 1.0339, and the other parameters are same as above. The radiation length of the medium is 0.16 micrometers if we consider the above situation (absorption length).

Using these sets of parameters and a computer program Figure 2.7 and Figure 2.8 were calculated from equation (2.15) Figure 2.7 corresponds to the carbon K edge, Figure 2.8 corresponds to the aluminum L2,3 edge. These figures represent power per unit solid angle at a particular frequency (at a particular Linac harmonic which is near the absorption edge frequency).

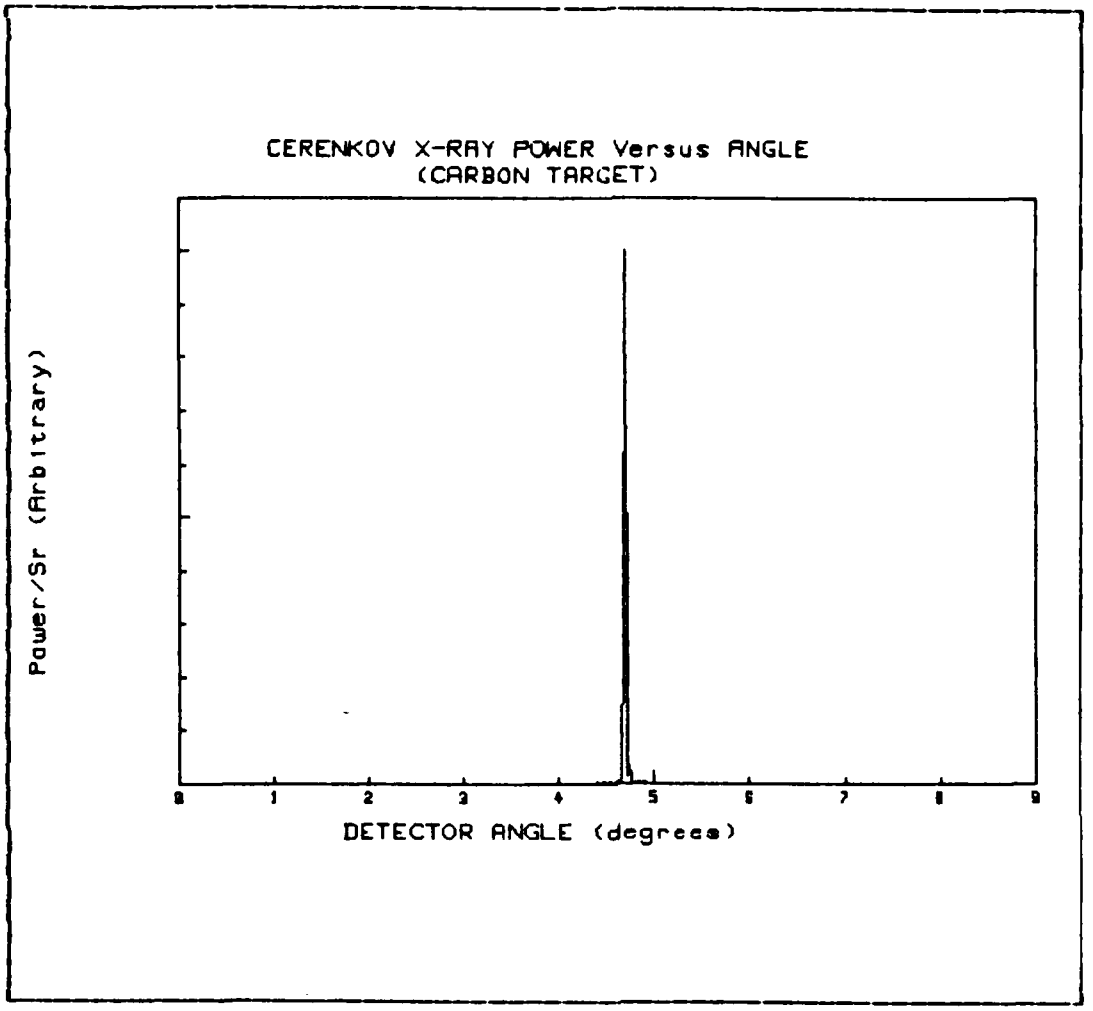

Figure 2.7 Power vs. Angle for Carbon Target.

For the case of large Z' (infinite medium), the total radiated power at frequency ω is given by

$$P_\omega = \frac{\mu}{4\pi}\omega v^2 \sin^2\theta_c \left|\hat{\rho}'_o(\vec{k})\right|^2 4\pi \frac{z'}{z^2} \qquad (2.20)$$

where ω is a harmonic of the bunch angular frequency ω_o, v is the electron velocity, θc is the Cerenkov angle, Z' is 1/2 of the pulse length or interaction distance, Z is spacing between electron bunches, and $\hat{\rho}'(\vec{k})$ is the three dimensional

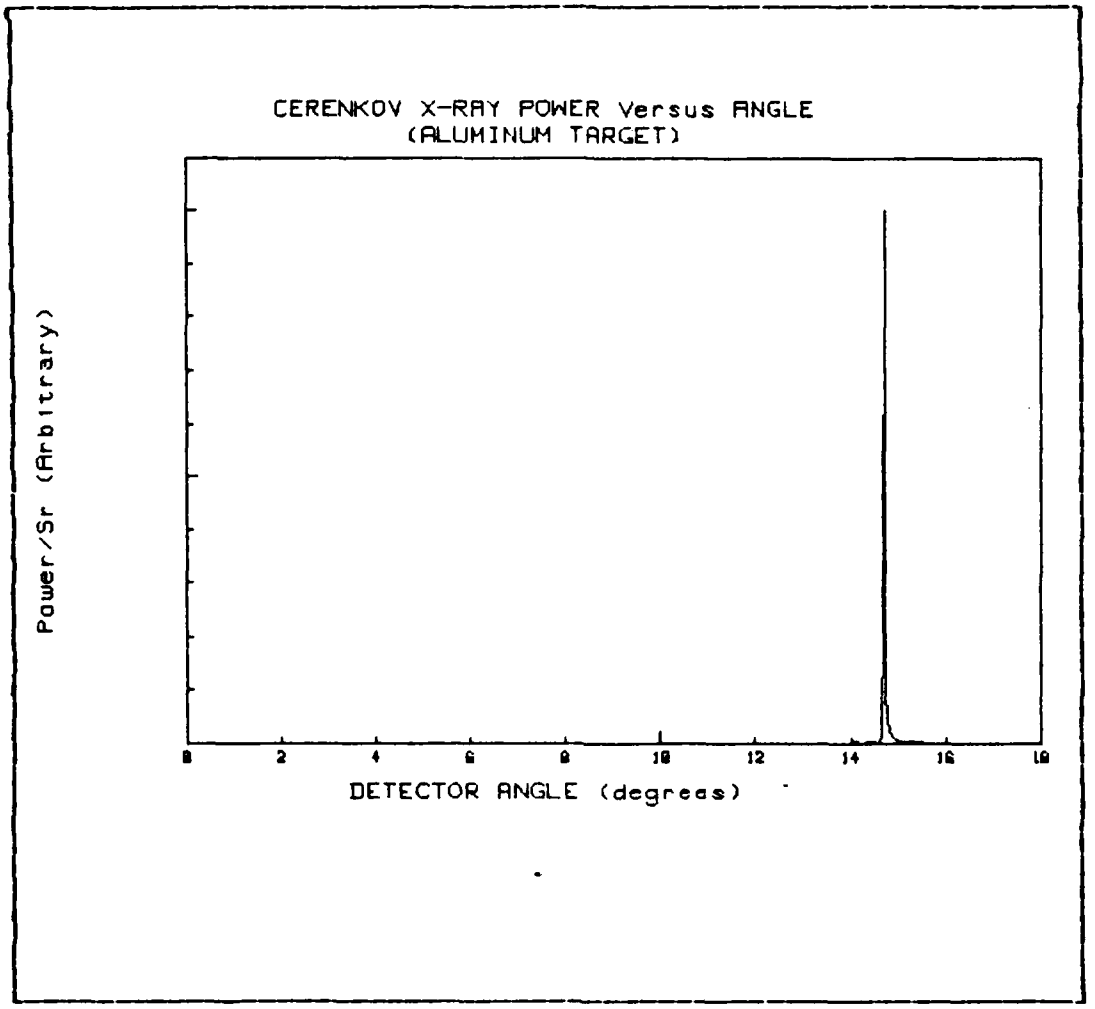

Figure 2.8 Power vs. Angle for Aluminum Target.

Fourier transform of the single pulse described by $\underset{\circ}{\rho}'(\vec{r})$. Now we recognize that the ratio of interaction distance to bunch spacing ($2Z'/Z$) is N, the number of bunches present in the interaction length. Also, the bunch spacing can be expressed as $Z = 2v/\omega_o$ where ω_o is the bunch repetition frequency. Making these substitutions, equation (2.20) becomes

$$P_\omega = \frac{\mu}{4\pi}\omega\omega_o V \sin^2\theta_c \left|\tilde{\underset{\circ}{\rho}}'(\vec{k})\right|^2 N \qquad (2.21)$$

To compare with usual formulations, equation (2.21) is divided by Nv to obtain the energy loss per unit path length per pulse. This gives

$$dE/dx = \frac{\mu}{4\pi} \omega \omega_o \sin^2\theta_c \left|\tilde{\rho}'_o(\vec{k})\right| \qquad (2.22)$$

where ω is a harmonic of the basic angular frequency ω_o of the periodic pulse train.

If the pulse is assumed to be a point charge, the Fourier transform $\tilde{\rho}'_o(\vec{k})$ reduces to q, the total charge per pulse, and equation (2.22) is very similar to the usual Cerenkov energy loss formula where for a single charge q, the radiation is continuous and the factor $\omega \omega_o$ in equation (2.22) is replaced by $\omega\, d\omega$.

$$dE/dx = \frac{\mu}{4\pi} \omega d\omega \sin^2\theta_c\, q_o^2 \qquad (2.23)$$

which is the classical formula derived by Frank and Tamm in 1937 [Ref. 1: p. 26]. In the case of a Linac the pulse train is periodic at angular frequency ω_o and radiation is emitted at the harmonic frequencies denoted by ω. The equation (2.23) shows that:

1. For an infinite medium, as would be the case for X-rays the radiation direction is at θ_c.
2. The intensity increases with ω.
3. The spectrum is continuous, ie, all frequencies are emitted.

Also from equation (2.23) and (2.2) we can calculate the energy radiated per unit length for one electron

$$E/1m = \frac{\mu}{4\pi} q_o^2 \int_{n\beta>1} \left(1 - \frac{1}{n^2(\omega)\beta^2}\right) \omega\, d\omega \qquad (2.24)$$

This calculation is done more in detail in Appendix A. From the results of Appendix A, we can now calculate the expected counting rate in a radiation detector. In all cases, we predict sufficient number of counts/sec to observe X-ray Cerenkov radiation. However, there is a danger that our

instaneous count rates may be too higher for our detector to respond properly. A solution to this effect is also predicted here. The number of photons per second detected by the proportional counter can be estimated by the following procedure:

1. From the results of the Appendix A, the radiated energy per unit length for a single electron is 1.48 x 10^{-14} Joule/m (ie. 9.25 x 10^{4} eV/m or 92.5 eV/mm) for the case of a carbon target, and dividing by the energy of one photon(284 eV) gives 0.3257 photons/mm emitted from the target (compare with the optical region 10 photons are emitted [Ref. 1: p. 22] for the case of water 1mm thickness).
2. Since the radiation emerging from the target is actually picked off the last layer having a thickness on the order of the absorption length the above value must be multiplied by the absorption length (0.40 micrometers for carbon). Remember photons which were emitted front side of the target would be absorbed and could not detected by the proportional counter. Thus 1.32 x 10^{-4} photons are emitted for one electron in the absorption length.
3. From the geometry of the detector chamber the solid angle can be calculated to be 1.7 x 10^{-4} steradians for the new designed detector chamber (remember the distance from the target to the proportional counter is 42 cm and the dimension of the window of the proportional counter is 3x10 mm). Including this effect 2.24 x 10^{-8} photons/electron could be detected by the proportional counter. However, the radiation is not emitted in a 4π solid angle but emitted as a Cerenkov cone and we detect a fraction of $2\pi r$ circumference(r = 5 cm for carbon K edge) of the base of the cone. From this consideration 4.20 x 10^{-6} photons/

electron could be detected by our proportional counter.

4. For a measured average SEM current of 1.0×10^{-8} Amp and the SEM efficiency of 6 %, 1.04×10^{12} electrons/sec are coming out the Linac. For this current 2.33×10^{4} photons/sec could be detected by our proportional counter if the photons are emitted in a 4π solid angle. For the more realistic case of emission into the $2\pi r$ circumference cone, 4.4×10^{6} photons/sec will be detected.
5. Furthermore, the number will be reduced by a factor of approximately 10 if we consider the efficiency of the proportional counter [Ref. 10] due to the thickness of the window(1000Å). If we follow the same procedure for the case of aluminum L-edge, we expect about 25 times stronger signal than carbon K-edge.
6. In reality, the pulse length of the Linac is approximately 1 μsec and the pulse repetition rate is 60 Hz. This means that the duty cycle is 6×10^{5} so the instantaneous current on the target is 2.78 mA for 1.67×10^{-7} Amp average current. As a consequence of this, the actual count rate during the measurement period by the proportional counter is 1.67×10^{4} higher than the average count rate in our consideration. When the experiment is done, it will be necessary to reduced the current so that the proportional counter can respond and is not saturated. One way to reduce the number of electrons/sec on the target is to turn off the gun grid of the Linac and run on the "dark" current which is the current of free electrons in the imperfect vacuum of the Linac which was accelerated by the RF fields.

Two other considerations which influence experimental observation are bremsstrahlung and multiple scattering. The bremsstrahlung cone angle is roughly

$$\langle\theta\rangle_{Brems} = 1/\gamma \qquad (2.25)$$

which is approximatly 0.3 degrees for 100 MeV electrons. For the carbon K edge and aluminum L edge the bremsstrahlung cone angle is much smaller than the Cerenkov cone angle. However the multiple scattering angle which is given approximately by

$$\langle\theta^2\rangle^{\frac{1}{2}} = (21/p\beta)\left[x/x_o\right]^{\frac{1}{2}} \qquad (2.26)$$

where x is the target thickness and x_o is the radiation length, p is the momentum of the electron in MeV/c. x_o is 18.8 and 8.9 cm for carbon and aluminum respectively. For 2.5×10^{-5} m carbon foil the multiple scattering angle is 0.14 degrees. In [Ref. 8] the aluminum target thickness was 2.5×10^{-5} m and the corresponding multiple scattering angle is 0.2 degrees. Both multiple scattering angles are much less than the Cerenkov cone angle. Target thickness must be kept small to keep bremsstrahlung and multiple scattering effects from masking Cerenkov effect.

Finally, for the experimantal geometry of Figure 3.2, the walls of the proportional counter will be closer to the beam than counter window. We must limit events due to secondary particles and bremstrahlung from fringe electrons in the beam striking the thick chamber walls. A small current is required for this reasion, in addition to the count rate considerations of item 6 above. Perhaps in Farmer's experiment [Ref. 8] the obserbed peak was due to a beam halo striking the proportional counter walls. A future facility should consider the installaticn of a damp magnet on the electron beam axis prior to the proportional counter in order to sweep away the electron beam.

In the case of X-ray Cerenkov radiation, at frequencies close to the absorption lines and bands of the medium, the

most substantial effect is absorption of virtual photons over the radiation formation length. For the X-ray region it is impossible to make bunching fine enough to see the radiation at harmonics of the bunch frequency. Furthermore, our medium is a thin film, but the wavelength of X-ray is even smaller in comparision with the thickness of the medium. Also, the index of refraction changes with frequency.

III. EXPERIMENTAL DESIGN AND PROCEDURE

A. EXPERIMENTAL APPARATUS

In this section, the components of the experimental apparatus will be examined in order to provide a precise understanding of the experiment. The various components of the signal train will be reviewed in order, from the originating device itself (Linac), to the final detection and analysis components.

1. Linac

The linear accelerator used for this experiment, see Figure 3.1, produces a bunched electron beam rather then a continuous one. Three klystron tubes are used to individually provide power to each of three ten foot long accelerating sections which are of the Stanford type. An electron gun at the beginning of the accelerator injects electrons at roughly $\beta = 0.5$. The design of the accelerator sections causes the RF energy to propagate in a TM mode. The injected electrons are quickly accelerated to near the velocity of light in their first few centimeters of travel. In order to narrow the energy spectrum, the highest energy electrons are separated from the others by bending the beam with a magnet, and then using a tungsten slit to block electrons not having the desired energy. As might be expected, the high energy electrons which impinge on the tungsten slit are the major source of gamma and X-ray radiation produced by the Linac. The Linac has the following operating characteristics; maximum energy of 120 MeV, maximum average current of 3-5 microAmp (measured by the secondary emission monitor), operating frequency of 2.856 GHz, and pulse duration of 1.0 microseconds.

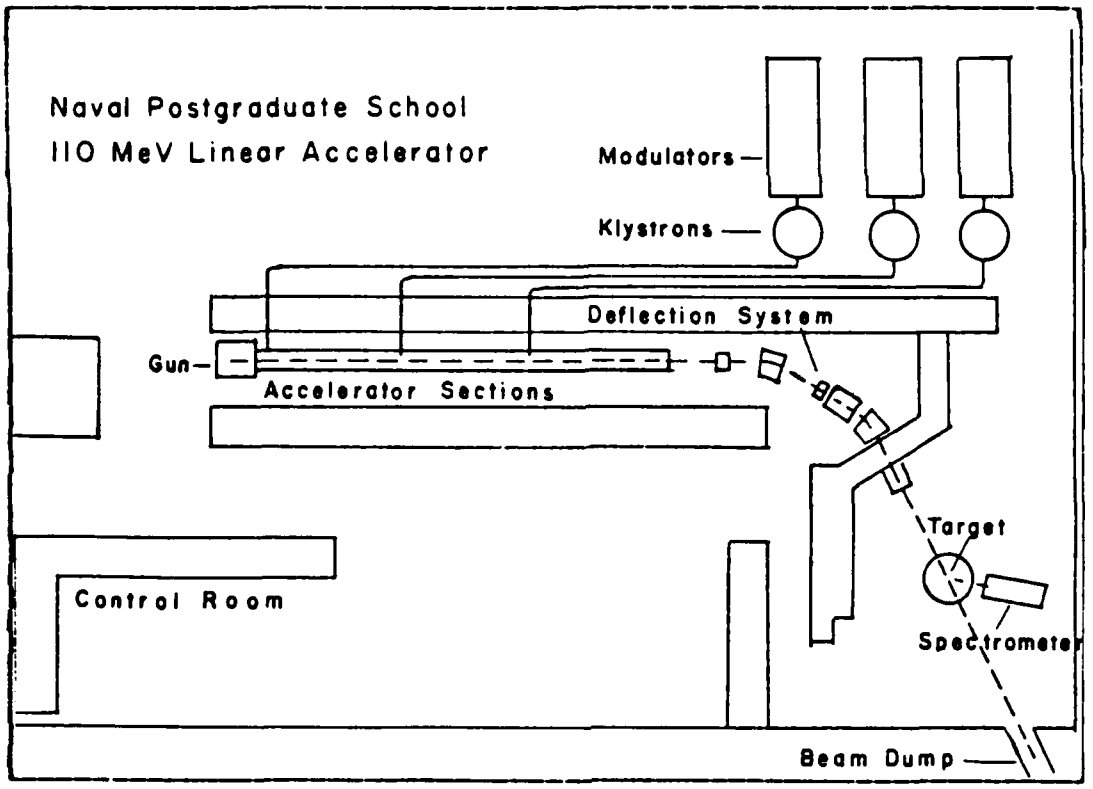

Figure 3.1 The Schemetic Diagram of a Linear Accelerator.

2. Target and Detector Chamber

The schemetic diagram of target and detector chamber which is made of aluminum is shcwn in Figure 3.2. During the experiment, the whole Linac, a target and detector chamber are under vacuum by using a mechanical pump and an oil diffusion pump. The pressure is about 10^{-6} Torr. Due to the characteristic of Cerenkov radiation and geometry of target and detector chamber, it is necessary to change the geometry of the target and detector chamber. This will be discussed carefully in the next section.

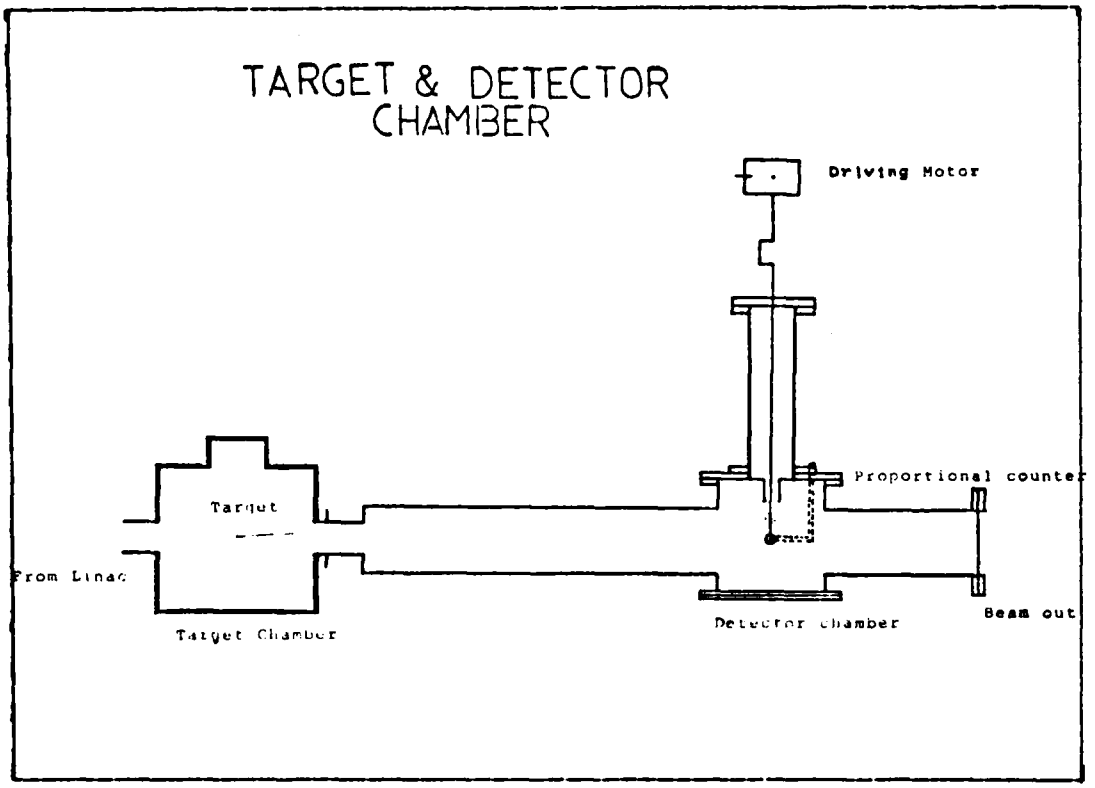

Figure 3.2 Target and Detector Chamber.

3. Gas Flow System

The schemetic diagram of the gas flow system for the proportional counter is shown in Figure 3.3. Vacuum pump 1 is always working during the experiment. If valve A is opened, then the pressure becomes the same in valves B,C and inside the proportional counter. Also, the target and detector chamber and the whole Linac become the same pressure (1st step). Now turn on vacuum pump 2, close valve A and open valve C and D, and introduce argon and methane gas mixture to the proportional counter by opening valve B (2nd step). In the first step, pressure meter A should read about 50 microns and pressure meter B about 760 mmHg. In the second step, pressure meter A remains the same but pressure

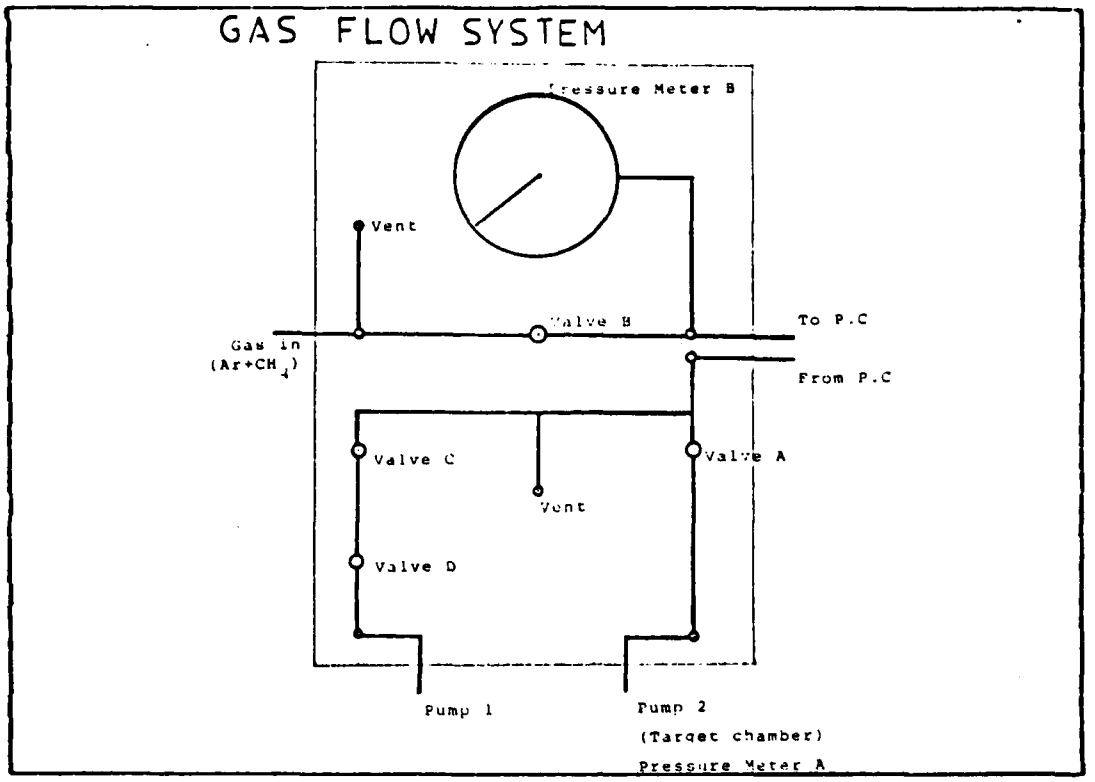

Figure 3.3 The Schemetic Diagram of a Gas Flow System.

meter B reads about 510 mmHg if the pressure of the proportional counter is 250 mmHg. Finally, supply high voltage to the proportional counter and find the optimum pressure and voltage of the proportional counter.

4. Detection Apparatus

In this section, the possible detection apparatus for the X-ray photon will be discussed. The Manson Model 04 gas flow proportional counter is shown in Figure 3.4. The cathode (body) is cylindrical in shape with an inner diameter of 2cm and overall length of 7cm. The anode consists of nichrome of 50 micrometer in diameter, and the window (1000 Å thickness) consists of VYNS, a co-polymer of vinyl

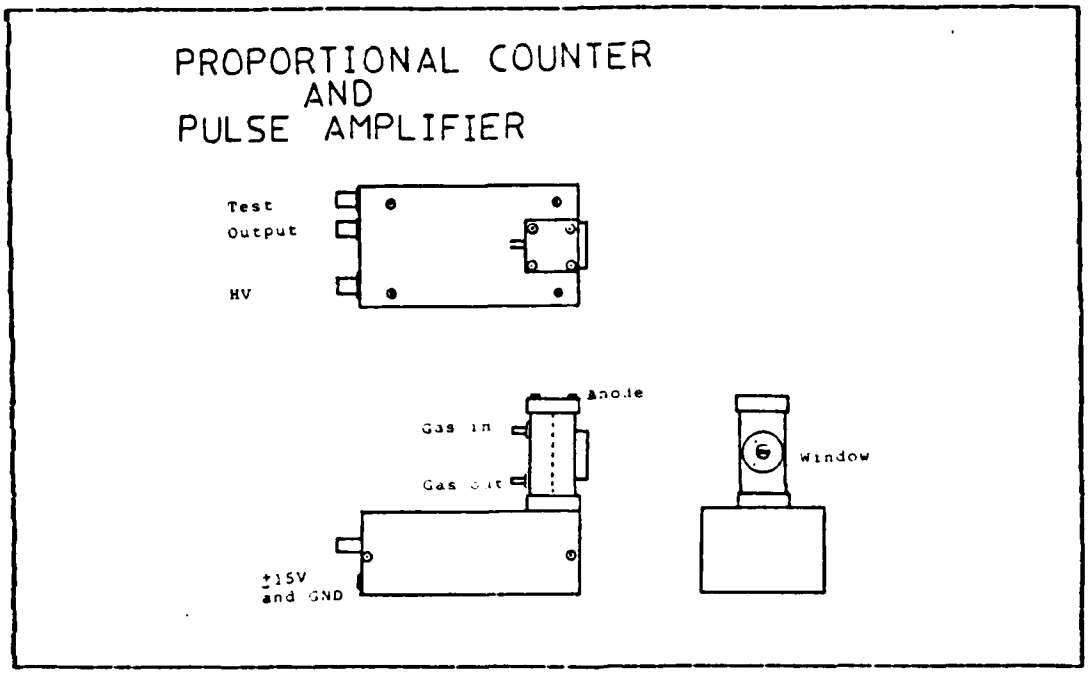

Figure 3.4 The Schemetic Diagram of a Proportional Counter.

chloride and vinyl acetate, with a 60 % transmission 400 mesh screen with a 3x10 mm slot for an operating differential pressure of about 800 Torr maximum. And for the proportional counter, gas mixture of 90 % argon and 10 % methane is provided by the gas flow system which was discussed before, and high voltage is supplied by the power supply.

The reason for the use of the flow-proportional counter is that the low energy photons generate just a few electron-ion pairs within this gas, and therefore the pulse formed has broad distributions extending down close to the amplifier noise level.

The proportional counter can be moved vertically by the driving moter, and the proportional counter is always pointed at the virtual center of the emission region.

The Manson Model PAL-01 pulse amplifier is shown in Figure 3.4. The input stage is a JFET-bipolar cascade, followed by quasi-Gaussian double differentiating and integrating filters with 0.75 μsec time constant. Its charge sensitivity is -2×10^{14} V/coul.

5. Observer Station

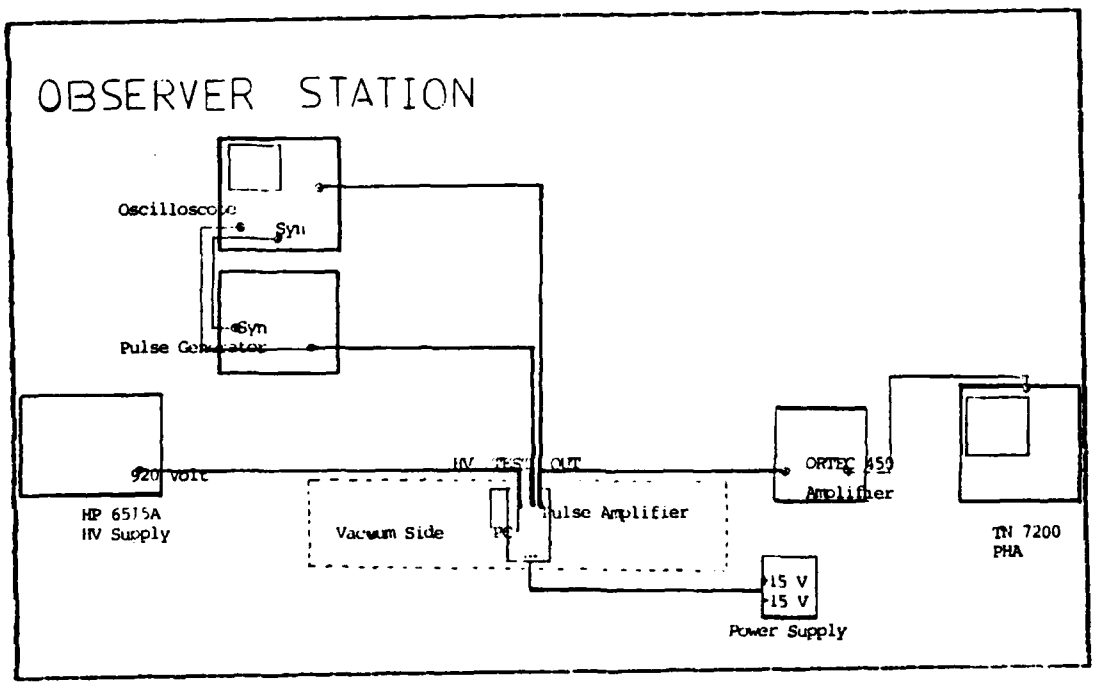

Figure 3.5 The Schemetic Diagram of a Observer Station.

As we see in Figure 3.5 the analyzing equipment consists of an ORTEC 450 Research Amplifier, a TEKTRONIX 7904A Oscilloscope, and a TRACER NORTHERN TN-7200 Pulse Height Analyzer (PHA). The impcrtant piece of equipment for this experiment was the PHA. This instrument divided the detection range into a predetermined number of channels (for example 1 K) and then recorded graphically the number of counts with which each signal channel was detected. The

data is presented in the form of pulse-height distribution with the number of counts per channel displayed on a linear vertical scale and the channel number displayed on a linear horizontal scale. The pulse-height is proportional to the incident photon energy. Thus the displayed results form an energy dispersed spectrum of the incident photon beam. This allowed the observer to deal with a certain degree of variability in the signal by choosing the observed value to be the peak of the frequency distribution.

B. BASIC EXPERIMENTAL DESIGN

1. General Considerations

TABLE II

Comparisions of Changing Design

Design	Length Tar-Det	Maximum Height	Maximum Angle
Original Design	114 cm	6.5 cm	3.6°
New Design Target(C)	72 cm	6.5 cm	4.8°
New Design Target(E)	42 cm	6.5 cm	8.8°

The purpose of this experiment is to measure the relative power from Cerenkov radiation as a function of detector angle in order to compare it with theoretical values. The electron bunches exit the Linac aperture (see Figure 3.1) and emit Cerenkov radiation when they go through the target (a thin film of carbon or aluminum). These

electrons pass the target and detector chamber and proceed into the beam dump, while the X-radiation emitted by Cerenkov mechanism travels to the detector chamber, making a Cerenkov cone, which is detected by the proportional counter. During the experiment the whole Linac and the target and detector chamber are under vacuum by a mechanical pump and an oil diffusion pump. The proportional counter is mounted in the detector chamber, which is placed such that the proportional counter is always pointed at the virtual center of the emission region.

With this experimental setup, the basic experimental procedure is to sweep the proportional counter vertically over the angular range of interest by using a small driving moter on the detector mount. The signal picked up by the proportional counter is amplified by the pulse amplifier which is mounted with the proportional counter(see Figure 3.4) and transmitted to the control room, where it is fed into an another amplifier and then into both an oscilloscope and a pulse hight analyzer (PHA). The oscilloscope allows a gross measure of power, while the number of counts measured by the pulse hight analyzer gives a more precise value. The end result of this procedure would be tabular data in the form of signal intensity versus detector angle.

2. The New Design of the Detector Chamber

As mentioned earlier, due to the characteristics of Cerenkov radition, it is hard to measure the angular dependance of relative power density with the original geometry of the detector chamber which was used by W.J Farmer [Ref. 8] Farmer was working with aluminum K-edge and measured 1.82° for Cerenkov angle but this experiment can not be repeated, notice the index of refraction of the aluminum K-edge is less than unity. However, if the electron beam axis was not exactly perpendicular to the proportional

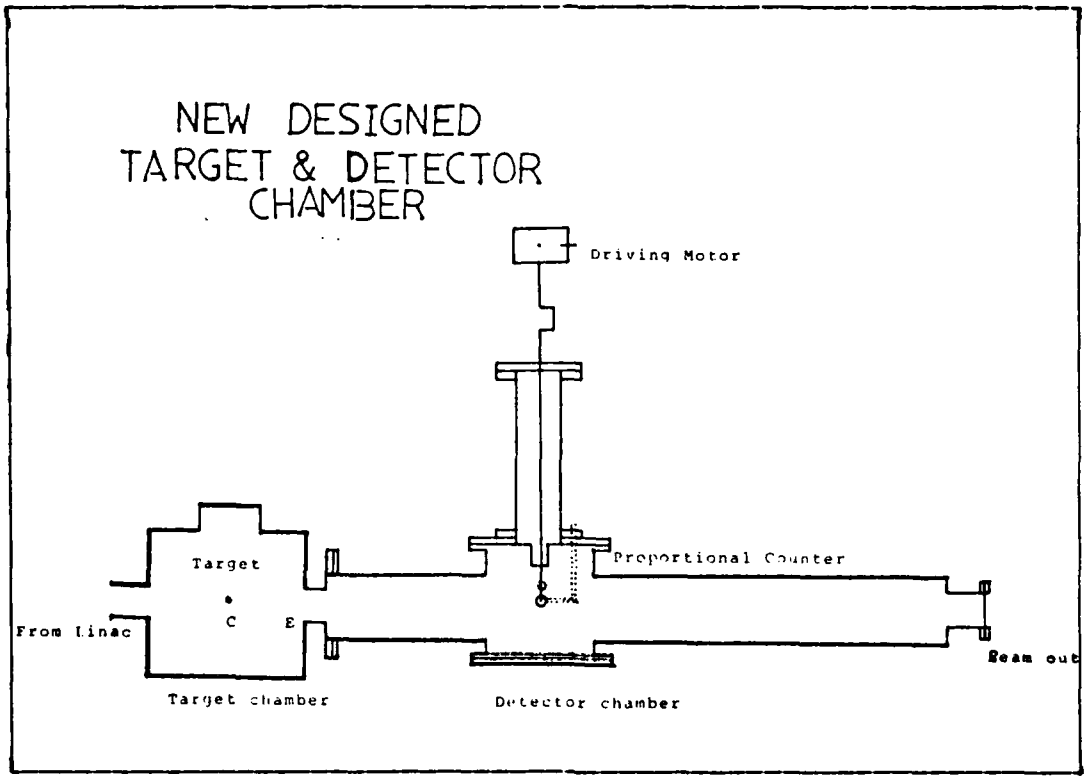

Figure 3.6 The New Design of Detector Chamber.

counter travel direction, it is possible that the L1 edge was detected. At this time, the exact interpretation of his result is difficult to assess.

From Table II, we observe that the old design allows a maximum Cerenkov cone angle of 3.6°. This corresponds to n = 1.002. If the prediction of Table I are not correct, in order for Cerenkov radiation from the K edge of aluminum to be observed, then the index of refrection must be $1.0 < n < 1.002$ at that frequency. Farmer measured $\theta c = 1.8$ degrees corresponding to n = 1.0005. If this was a correct measurement, and Table I is incorrect, then the measurement should have been able to be repeated. We suspect that the original measurements were not complete and something other then Cerenkov radiation was observed.

Because the Cerenkov cone is large, the edge of the detector chamber will interrupt the radiation. Hence it is necessary to reduce the length of the detector chamber to enable it to detect at a much larger angle. Also, the detection angle can be made larger if the target is placed at the exit(E) of the target chamber rather then at the center(C). The new design of the detector chamber is shown in Figure 3.6, and comparisions are sumarized in Table II.

C. PROCEDURE

To prove the theories presented in this thesis, the following Cerenkov X-ray experiments are considered. They utilize absorption edges as follows:

1. Carbon K (283.84 eV) (experiment #1).
2. Aluminum L1 (87.01 eV), L2,3 (72.78 eV) (experiment #2).
3. Aluminum K (1559.9 eV) (experiment #3).

TABLE III

Cerenkov Angle for 100 MeV Electrons

Target Material	Threshold Energy in MeV	Index of Refraction (n)	Cerenkov Angle (θ_C)
Carbon K edge	6.23	1.003379	4.694°
Aluminum L1 edge	4.89	1.0055	5.988°
Aluminum L2,3 edge	2.01	1.0339	14.713°
Aluminum K edge	No	0.99992	No

Also, the corresponding index of refraction(n) and calculated Cerenkov angle(θc) using equation (2.2) for 100 MeV electrons are tabulated in Table III. We see that Cerenkov angle(θc) is large compared with the geometry of target and detector chamber.

In the original experiments of V.A. Bazylev et. al. [Ref. 3: p. 884] a carbon target was used. The work was performed with a linear accelerator at an electron energy of 1.2 GeV.

Here, for experiment #1 the target consisted of a plate of graphite carbon with density 1.75 g/cm^3, transverse dimensions of 4x4 cm and thickness of 126 micrometers, and for experiments #2, #3 an aluminum foil with density 2.67 g/cm^3, transverse dimensions of 4x4 cm and thickness of 200 micrometers could be used.

On the basis of the calculations performed, maximum Cerenkov X-ray photons should be observed at the angle near 4.694 for the case of the experiment #1 (carbon K edge) and 5.988 for the experiment #2 (aluminum L1 edge) and with the present apparatus, the aluminum L2,3 edge should not be observable. As described in section B, the geometry of target and detector chamber needs to be changed, and also the target material must be placed at the exit(E) of target chamber rather then at the center(C) of the target chamber (see also Figure 3.6 and Table II).

The Naval Postgraduate School's Linear accelerator (LINAC) is capable of producing relativistic electrons with energies of 100 MeV. The electrons are accelerated to energies of 100 MeV which are passing through the target material and produce Cerenkov radiation. This process occurs in a vacuum chamber. Exiting Cerenkov X-radiation then travels a distance of 42 cm, within a vacuum chamber from the target material to the proportional counter within another evacuted chamber. The proportional counter is

suspended from the top of the detection chamber by a support cylinder which is moveable in the vertical direction. The full movement of the cylinder allows the counter to traverse a distance of 13 cm, or an angle of 17.20 degrees.

In the W.J. Farmer experiments [Ref. 8] in working with the same experimental apparatus which are discussed in section A the proportional counter was filled with gas at pressure of 250 Torr. The gas mixture was 90 % argon and 10 % methane. The bias voltage on the detector was 920 volts.

In preparing for the experiment, the proportional counter was calibrated by utilizing an iron 55 sample to produce 5.89 KeV X-radiation within the evacuated detector chamber. As a result of the radiation from the calibration source, the K edge of argon was excited at 3.2 KeV. These two energies provided two points at which the PHA used in this experiment could be calibrated.

It was noted during the course of the calibration of the detector that the proportional counter was very sensitive to change in gas pressure and bias voltage.

IV. RESULTS AND DISCUSSIONS

Due to repeated failure of the preamplifier (when high bias voltage is applied to the proportional counter a break down occurs on the circuit board of the preamplifier during bench tests to characterize the proportional counter response characteristic) no measurement of X-ray Cerenkov radiation was made. It seems to be a design problem of the preamplifier.

A preamplifier is specifically designed to accept the signal from a detector with minimum shaping in order to preserve the maximum signal-to-noise ratio. The three basic types of preamplifiers that are normally used are voltage sensitive, current sensitive, and charge sensitive. Charge sensitive preamplifiers are preferred for most spectroscopy applications. ORTEC model 142PC and 142IH preamplifiers could be used for this experiment. These are low-noise, high-gain charge sensitive units designed for use with proportional counters.

This thesis showed that Cerenkov X-radiation is obtainable. More work needs to be done theoretically to support the results of this experiment by evaluating the real part of the index of refraction in the vicinity of the absorption edge of target material and using it in the presented equations to determine the theoretical values of the Cerenkov angle and the energy of the X-radiation relased.

More work should also be done to see if there are other elements which will produce Cerenkov X-radiation at some other energy. These radiation, if found, could be utilized as monoenergetic sources for lithographic studies or any other studies in which a monoenergetic X-ray source would be desirable. X-ray lithography is an important alternative to

optical and ultraviolet lithography because it overcomes problems of penumbral and geometric distortion which impose severe constraints on mask to wafer positioning. The Cerenkov X-ray sources are highly directional and there is even less distortion than a conventional X-ray source. There has also been a discussion of the possibility of pumping nuclear and electronic levels by X-radiation with the goal of developing X-ray lasers.

Several advantages [Ref. 9] of a Cerenkov radiation are:

1. The emission is in a narrow cone, with a small cone angle. This means that all the radiation can be collected and tightly focused.
2. Operation is in relatively low vacuum (about 10^{-3} Torr), in contrast with the 10^{-7} - 10^{-12} Torr pressure for the synchrotron radiation.
3. For an electron beam with energy greater than the threshold energy, it is relatively simple to obtain Cerenkov radiation. No magnetic field is required, as in synchrotron radiation.
4. Cerenkov radiation in the X-ray region has a relatively small spectral width and therefore is quite monochromatic.

APPENDIX A

NUMERICAL CALCULATION OF THE EQUATION (2.24)

```
1000  !"ALUMINUM  " 11-6-1984
1010  ! This is a basic HP language program which calculates the
1020  ! energy radiated per unit length for one electron for the
1021  ! case of aluminum L edge and carbon K edge.
1030  ! PROGRAM SOLVES FOR RADIATED ENERGY PER UNIT LENGTH
1040  !                FOR SINGLE ELECTRON
1050     DIM Array(27,2)
1090     FOR K=1 TO 2
1100        IF K=1 THEN PRINT "      ALUMINUM"
1110        IF K=2 THEN PRINT "      CARBON"
1120        READ Points
1140        REDIM Array(Points,2)
1141        PRINT
1142        PRINT "      OMEGA          n"
1143        PRINT
1150        FOR I=1 TO Points
1160           FOR J=1 TO 2
1170              READ Array(I,J)
1171              PRINT USING "#,K";"  "
1180              PRINT USING "#,D.DDDDESZZ";Array(I,J)
1190           NEXT J
1200           PRINT
1210        NEXT I
1230        Sumde=0
1240        PRINT
1250        PRINT " DOMEGA     dE/dX                  SUMdE"
1260        FOR I=2 TO Points
1270           Domega=Array(I,1)-Array(I-1,1)
1280           F1=Array(I-1,1)*(1-1/(Array(I-1,2)*.999986943)^2)
1290           F2=Array(I,1)*(1-1/(Array(I,2)*.999986943)^2)
1300           Dedx=2.5587021891E-45*Domega*(F1+F2)/2.
1310           Sumde=Sumde+Dedx
1320           PRINT Domega,Dedx,Sumde
1330        NEXT I
1331        PRINT
1333        PRINT " RADIATED ENERGY PER UNIT LENGTH "
1334        PRINT " FOR SINGLE ELECTRON(Joule/meter):"
1340        PRINT "      ",Sumde
1350        PRINT USING "@"
1360     NEXT K
1390     STOP
```

```
1400 Alum:DATA 27, 1.032E17,1.0011, 1.047E17,1.0034, 1.063E17,1.0062,
1410      DATA      1.078E17,1.0100, 1.093E17,1.0163, 1.108E17,1.0243,
1420      DATA      1.123E17,1.0146, 1.139E17,1.0113, 1.154E17,1.0101,
1430      DATA      1.169E17,1.009,  1.184E17,1.072,  1.199E17,1.0069,
1440      DATA      1.214E17,1.007,  1.230E17,1.0071, 1.245E17,1.0071,
1450      DATA      1.259E17,1.007,  1.275E17,1.0069, 1.290E17,1.0065,
1460      DATA      1.306E17,1.0059, 1.321E17,1.0055, 1.336E17,1.0054,
1470      DATA      1.351E17,1.0056, 1.366E17,1.0054, 1.381E17,1.0048,
1480      DATA      1.397E17,1.0039, 1.412E17,1.0024, 1.427E17,1.0005,
1490 Carbon:DATA 4,4.279E17,1.00042,4.294E17,1.00084,4.310E17,1.0017,
1491         DATA   4.325E17,1.00338,
1500      OUTPUT 2 USING "#,K";C$
1510      PRINT "Continue working, You are back in the BASIC System."
1520      END
```

As a results of the calculations the energy radiated per unit length for one electron are:

1. 1.48×10^{-14} Joule/m (ie. 9.25×10^{4} eV/m) for carbon K-edge.
2. 2.35×10^{-13} Joule/m (ie. 1.47×10^{6} eV/m) for aluminum L-edge.

APPENDIX B
LITERATURE SEARCH FOR CERENKOV RADIATION

A literature search was done at the Naval Postgraduate School Library. The following database were searched: INSPEC, SPIN, COMPENDEX and ENGINEERING MEETINGS. The INSPEC database is the largest English language database in the fields of physics. The total number of journals scanned is over 2,000 and 200 of these are abstracted completely.

There are 123 articles related to Cerenkov X-radiation (among them many articles are related to astrophysics) 7 of which are useful for the X-ray Cerenkov experiment discussed in this thesis:

1. Bazylev, V.A "Line Shape of Spontaneous Cerenkov Radiation in the X-ray Region. Theory of Stimulated Radiation."
2. Rynne, T.M "Synchrotron Cerenkov Radiation in the Vicinity of an Atomic Absorption Edge."
3. Bazylev, V.A "Intense Electromagnetic Radiation from Relativistic Particles."
4. Piestrup, M.A "Cerenkov Radiation as a Light Source for the 2,000-620 Å Spectral Range."
5. Kolpakov, A.V "Vavilov-Cerenkov Effect in the X-ray Range."
6. Bazylev, V.A "X-ray Cerenkov Radiation. Theory and Experiment."
7. Gilmore, R.S "An Observation on the Spatial Distribution of Vacuum UV Photons Generated by Cerenkov Radiation."

LIST OF REFERENCES

1. Jelly, J.V., "Cerenkov Radiation and Its Applications" Pergammon, London, 1958.

2. Kolpakov, A.V., "The Vavilov-Cerenkov Effect in the X-ray Wavelength Region", Soviet Journal of Nuclear Physics, vol. 16, pp. 554-555, May 1973.

3. Bazylev, V.A., et al., "X-ray Cerenkov Radiation. Theory and experiment", Soviet Physics JETP, vol. 54, pp. 884-892, November 1981.

4. Zhevago, N.K., "Loss of Energy by an Electron with Periodic Inhomogenities", Soviet Physics JETP, vol. 45, pp. 224-228, February 1977.

5. Henke, B.L., et al., "Atomic Data and Nuclear Data Tables" Academic Press, vol. 27 January 1982.

6. Smith, D.Y., et al., "The Optical Properties and Complex Dielectric Function of Metallic Aluminum from 0.04 to 10 eV", Argone National Laboratory, March 1983.

7. Buskirk, F.R. and Neighbours, J.R., "Cerenkov Radiation from Periodic Electron Bunches", Physical Review A, vol. 28, pp. 1531-1538, September 1983.

8. Farmer, W.J, Cerenkov Radiation in the X-ray Region, M.S Thesis, Naval Postgraduate School, Monterey California, March 1984.

9. Piestrup, M.A., et al., "Cerenkov Radiation as a Light Source for the 2000 Å - 620 Å Spectral Range", Applied Physics Letters, vol. 28, pp. 92-94, January 1976.

10. Manson, J.E., "Instructions for Model 04 Photon Counter", Private Communication, February 1984.

INITIAL DISTRIBUTION LIST

		No. Copies
1.	Professor F. R. Buskirk, Code 61Bs Department of Physics, Naval Postgraduate School, Monterey, California 93943	2
2.	Professor J. R. Neighbours, Code 61Nb Department of Physics, Naval Postgraduate School, Monterey, California 93943	5
3.	Professor X. K. Maruyama, Code 61Xa Department of Physics, Naval Postgraduate School, Monterey, California 93943	5
4.	Physics Library, Code 61 Department of Physics, Naval Postgraduate School, Monterey, California 93943	2
5.	Defense Technical Information Center, Cameron Station, Alexandria, Virginia 22314	2
6.	Library, Code 0142, Naval Postgraduate School, Monterey, California 93943	2
7.	Major Youn Dae Choi, Jangsoon Ri 511, Jeungwoo Myun, Jeungeub Gun, Chunrabuk Do. 561-83, Republic of Korea	1
8.	Major Youn Dae Choi, Daebong Apt B-209, Daebong Dong Il Gu 55-149, Taegu. 634, Republic of Korea	2

END

FILMED

6-85

DTIC